Journal of Radiation Research, 2013, 54, 146–151
doi: 10.1093/jrr/rrs055 Advance Access Publication 22 July 2012

Simulation approach for the evaluation of tracking accuracy in radiotherapy: a preliminary study

Rie TANAKA[1,*], Katsuhiro ICHIKAWA[1], Shinichiro MORI[2] and Sigeru SANADA[1]

[1]Department of Radiological Technology, School of Health Sciences, College of Medical, Pharmaceutical and Health Sciences, Kanazawa University, 5-11-80 Kodatsuno, Kanazawa, 920-0942, Japan
[2]Research Center for Charged Particle Therapy, National Institute of Radiological Sciences, 4-9-1 Anagawa, Inage-ku, Chiba, 263-8555, Japan
*Corresponding author. Tel: +81-76-265-2537; Fax: +81-76-234-4366; E-mail: rie44@mhs.mp.kanazawa-u.ac.jp

(Received 25 February 2012; revised 18 May 2012; accepted 18 June 2012)

Real-time tumor tracking in external radiotherapy can be achieved by diagnostic (kV) X-ray imaging with a dynamic flat-panel detector (FPD). It is important to keep the patient dose as low as possible while maintaining tracking accuracy. A simulation approach would be helpful to optimize the imaging conditions. This study was performed to develop a computer simulation platform based on a noise property of the imaging system for the evaluation of tracking accuracy at any noise level. Flat-field images were obtained using a direct-type dynamic FPD, and noise power spectrum (NPS) analysis was performed. The relationship between incident quantum number and pixel value was addressed, and a conversion function was created. The pixel values were converted into a map of quantum number using the conversion function, and the map was then input into the random number generator to simulate image noise. Simulation images were provided at different noise levels by changing the incident quantum numbers. Subsequently, an implanted marker was tracked automatically and the maximum tracking errors were calculated at different noise levels. The results indicated that the maximum tracking error increased with decreasing incident quantum number in flat-field images with an implanted marker. In addition, the range of errors increased with decreasing incident quantum number. The present method could be used to determine the relationship between image noise and tracking accuracy. The results indicated that the simulation approach would aid in determining exposure dose conditions according to the necessary tracking accuracy.

Keywords: noise simulation; image noise; flat-panel detector (FPD); target tracking; radiotherapy

INTRODUCTION

Dynamic flat-panel detectors (FPDs) are commonly used in clinical practice. In external radiotherapy, real-time tumor tracking can be achieved by diagnostic (kV) X-ray imaging with a dynamic FPD [1–3]. There is concern regarding the relationship between image quality and accuracy of target tracking, because low image quality is associated with the risk of increased tracking errors, although it can reduce the patient dose. There are a number of factors that affect image quality, such as X-ray tube voltage, radiation dose and patient body shape. In particular, reducing the radiation dose leads directly to an increase in image noise, and this may be one of the major factors reducing the accuracy of target tracking.

Recently, several methods for measuring the temporal modulation transfer function (MTF) and the detective quantum efficiency (DQE) have been proposed, and the properties of FPDs used in dynamic imaging have been reported [4–7]. There are several reports on the performance of electric portal imaging devices [8–9]. In a previous study, it was revealed that a patient dose could be reduced by approximately 28% by optimal settings for the low-dose acquisition mode with respect to image quality and dose [10]. However, there have been no studies regarding the effects of image noise on tracking accuracy. It is necessary to address the relationship between image noise and accuracy of target tracking to keep the patient dose as low as possible while maintaining tracking accuracy.

A number of researchers reported on methods for simulating reduced dose images. The technique provides reduced dose images by adding white Gaussian noise with a certain standard deviation to the original image [11–14]

or by adjusting noise power spectrum (NPS) and DQE [15–16]. In general, X-ray images have image noise due to statistical fluctuations in the number of incident quanta entering a detector (q) [17–18]; a higher quantum number results in less image noise. The value of q is determined as the reciprocal of the Wiener spectrum (WS) of the system (i.e. $q = 1/\mathrm{WS}$), which is measured in flat-field images. The relationship between q and pixel value in an image is also determined from the average pixel value in the region of interest (ROI), where the WS was measured. Furthermore, q follows a Poisson distribution. Thus, images with various noise levels can be simulated by changing the value of q and inputting the values into a Poisson random number generator. The simulation images allow us to evaluate the accuracy of target tracking at any noise level and to determine the appropriate exposure dose. We evaluated the accuracy of target tracking in simulation images with various noise levels. Our purpose was to develop a computer simulation method to determine imaging conditions during target tracking in radiotherapy. We developed a computer simulation platform based on a noise property of the imaging system and investigated the feasibility of the simulation approach.

MATERIALS AND METHODS

Measurement of noise power spectrum (NPS)

Image data set

A set of images was generated for determination of the NPS of a direct-type (a-Se/TFT) FPD system (SONIALVISION Safire2; Shimadzu, Kyoto, Japan). The system was developed for real-time target tracking in 3D for external radiotherapy, and two detectors were orthogonally-placed at 1.0 m in the source-to-image distance (SID). In this study, one of the FPDs was examined. An RQA5 X-ray spectrum was used (HVL = 7.1 mm Al, realized with 21 mm Al additional filtration at 70 kV) [19]. The matrix size was 2048×2048 pixels, the pixel size was 0.123×0.123 mm and the field of view was 25.4×25.4 cm. Image preprocessing consisted of offset and gain correction as well as compensation for defective or nonlinear pixels, as applied in normal clinical use of the detector. Pixel scaling was linear with respect to exposure, with a bit depth of 16 bits.

NPS determination methods

For determination of the NPS, three independent flat-field images were obtained at each of two exposure levels (six images in total); the exposure levels (air kerma) were 7.54 μGy and 15.7 μGy, respectively, for the two series. The air kerma values were measured free-in-air in the detector plane with an ionization chamber (AE-132a 2902209; Oyogiken Inc., Tokyo, Japan). The SID was limited to 1.0 m in the system evaluated. The ionization chamber was placed 500 mm behind the detector, which was located approximately halfway between the X-ray tube and the detector surface. The air kerma at the detector surface was calculated by the inverse square distance law.

Regions of interest (ROIs), located manually near the detector center, were 256×256 pixels in size, with a pixel sampling pitch of 0.123 mm, in the same subarea of the full detector area, for the two series. Average pixel values were measured by use of Image-J ver. 1.42 [20] in each ROI. The NPS was calculated according to IEC6220-1-1 [21]. For removing long-range background trends, a 2D second order polynomial was fitted to each image and subtracted. The area of each image was divided into half-overlapping ROIs for each image and the results were averaged. The 2D NPS was then calculated by application of the fast Fourier transform to each ROI. One-dimensional cuts through the 2D NPS were obtained by averaging of the central ± 7 lines (excluding the axis) around the horizontal and vertical axes [22].

Creation of conversion function from pixel value to quantum number

The q is determined as the reciprocal of the WS [mm^2] of the system as follows [17–18]:

$$q = \frac{1}{WS} \tag{1}$$

In the present study, to determine q using Eq. (1), the averaged WS through all spatial frequencies in two directions was used as WS in Eq. (1) for each exposure level. The quantum number per pixel q' was then derived as follows:

$$q' = q \times ps \times ps \tag{2}$$

where ps is the pixel size, which was 0.123 mm in this study. The average pixel value (in digital units) vs the number of incident quanta (in count units) was fitted with a linear function, $y = \mathrm{a} + \mathrm{b}x$

Simulation of image noise

In this preliminary study, we simulated image noise by using a simplified method based on statistical fluctuations in the number of incident quanta entering a detector [11–14]. Although there is a limitation to simulating image noise with high accuracy, it was confirmed that the method would give promising results for simulating image noise under different dose levels.

A tracking implanted marker (home-made metal material) with an acrylic plate 20 cm thick was located in clinical settings during target tracking in radiotherapy and was imaged at the imaging conditions used clinically in our institution, 70 kV, 250 mA, 36 ms, and SID = 1.0 m. An averaging image was then created from ten images obtained at the above dose as a substitute for the image with vanishingly low image noise obtained with a large dose.

Pixel values were converted to quantum number according to the conversion function. Subsequently, the resulting image was weighted from 0.1 to 1.0 in increments of 0.1. Image noise was induced by statistical fluctuation of the quantum incident to the detector, which followed a Poisson distribution. The expected value of a Poisson-distributed random variable is equal to the mean and variance. Signal to noise ratio is defined as $\sqrt{q}$ (= $q/\sqrt{q}$) and thus a higher quantum number q results in less image noise [14, 17–18]. Thus, to simulate image noise, the weighted images were input into the Poisson random number generator in each pixel. The output was the final resulting image with image noise.

Data analysis

Target tracking

The targets in the simulation images were tracked by a template-matching technique [23]. The sum of differences in pixel value (R) between the search area in the next frame, S $(x+dx,\ y+dy)$, and the template in the current frame, T $(x,\ y)$, was expressed as follows:

$$R = \sum_{y=0}^{N}\sum_{x=0}^{M} |S(x+dx, y+dy) - T(x,y)|$$

$$(0 < x < M, 0 < y < N, -10 < dx < 10, -10 < dy < 10) \quad (3)$$

M and N are the size of the template, and dx and dy are the search range. The smallest R value was obtained when there were more similarities in the search area and template. The amount of shift (dx, dy) in the search area was determined by minimizing R, and the coordinates after movement were expressed as $(x+dx,\ y+dy)$. In this study, the initial template was given as a region into which the target was inserted in the first frame. After the second frame, the matching region of interest in the previous frame was used as the new template. The size of the template was 50×50, the search range was ± 10 pixels, thus the search area was 70×70 pixels, determined to cover the displacements of implanted targets.

Evaluation method

Tracking accuracy was evaluated in images at 10 different simulated noise levels. The implanted marker was shifted in known amounts by image processing, ± 3 and ± 6 pixels in the superior-inferior and right-left directions, respectively. A total of nine patterns were assessed for each noise level, as shown in Fig. 1. The coordinates tracked were compared to the known shift amounts, and the differences were calculated as tracking errors. The maximum tracking errors were calculated and compared between simulation images at different levels of image noise.

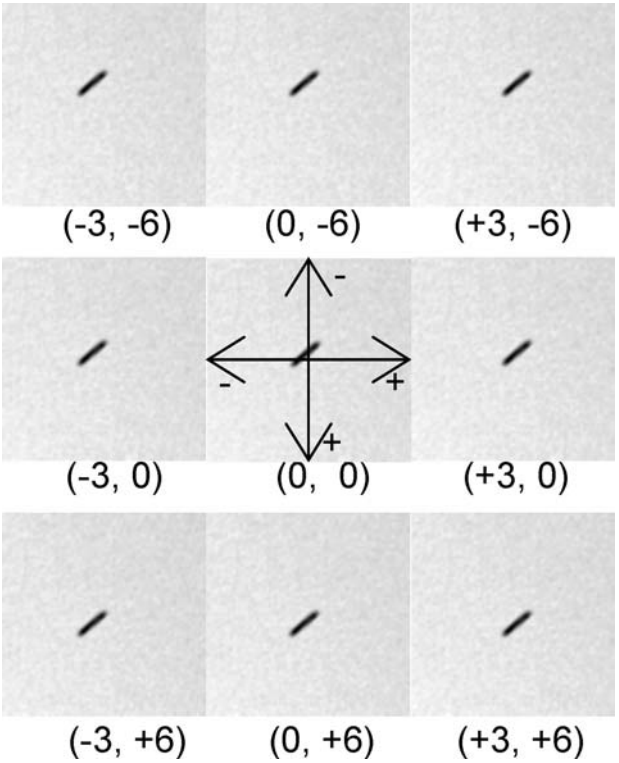

Fig. 1. Markers were shifted in nine combinations of ± 3 and ± 6 pixels in superior-inferior and right-left directions, respectively.

RESULTS

NPS properties

Figure 2 shows the WS in the horizontal and vertical directions for two exposure levels. The results indicated that the present system had a stable WS through all spatial frequencies, reflecting the noise property of a direct-type of FPD. A high exposure level resulted in a lower WS than a low exposure level at all of the spatial frequencies in both horizontal and vertical directions.

Conversion function from pixel value to quantum number

The average WS through all special frequencies of two directions in 7.54 μGy and 15.7 μGy were 9.57×10^{-6} mm^2 and 5.83×10^{-6} mm^2, respectively. Thus, the quantum numbers q at each exposure level were 1.05×10^{-5} mm^{-2} and 1.71×10^{-5} mm^{-2}, respectively, according to Eq. (1). The quantum numbers per pixel q' were 1.58×10^{-3} pixel^{-2} and 2.59×10^{-3} pixel^{-2}, respectively, according to Eq. (2). The fitted parameters values were a = 0.0585 digital units and b = 541.35 digital units per count. The quantum number per pixel q' was not zero even when the pixel value was zero due to system noise caused by the electrical circuit and system.

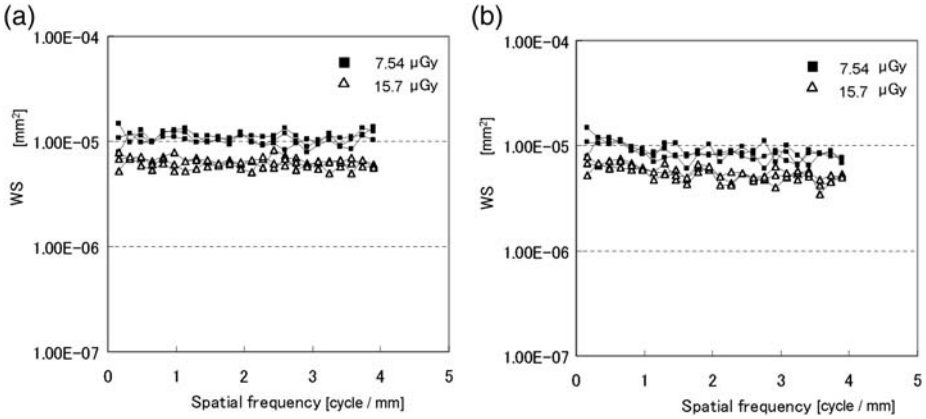

Fig. 2. Noise power spectra as determined for the set of flat-field images at two noise levels. (**a**) Horizontal direction. (**b**) Vertical direction.

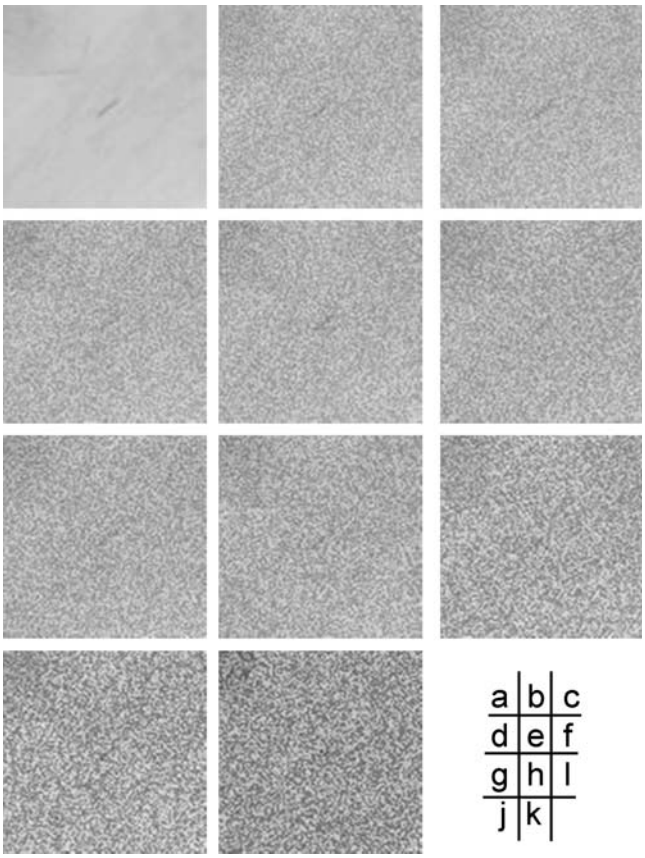

Fig. 3. Simulation images at 10 different noise levels. (**a**) Averaging image (i.e. image without noise). (**b**)–(**k**) Images with simulated noise achieved by decreasing the number of incident quanta by 10%. Image noise increased as the incident quantum number decreased.

Effects of image noise on target tracking

Figure 3 shows the simulation images at 10 different noise levels. The results indicated that a lower quantum number resulted in more image noise. It was difficult to recognize the location of the marker at quantum numbers <40%. Figure 4 shows the results regarding automatic tracking of implanted markers. There was no error in the average images without noise. The maximum tracking error increased with decreasing incident quantum number, as shown in Fig. 4. In the specific settings examined in this study, the tracking error tended to increase at less than half of the original quantum number. Error bars show the standard deviation of nine data sets ($n = 9$). The range of errors also became larger in simulation images created with smaller incident quantum numbers.

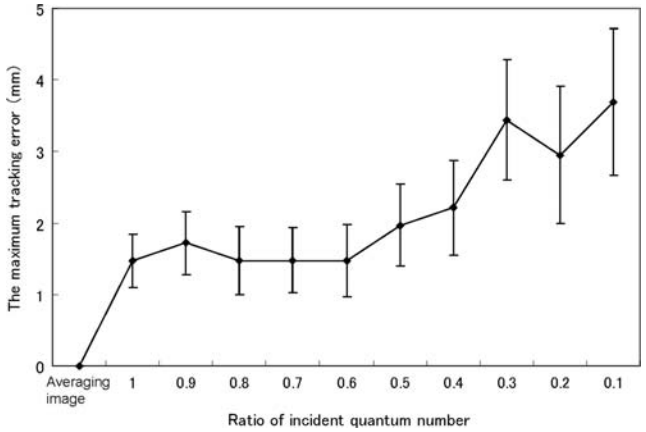

Fig. 4. Relationship between the maximum tracking error and ratio of incident quantum number to FPD (flat-field image). The average image without noise has no error, while there are tracking errors in the images simulated in ratio of incident quantum number from 1.0 to 0.1. Error bars show ±SD. (SD = standard deviation, $n = 9$).

DISCUSSION

Image noise has a big effect on visualization of an object with low contrast like a target in radiotherapy. The present

method was able to provide the relationship between image noise levels and tracking accuracy, although it is a specific parameter setting. The maximum tracking error increased with increases in the image noise. The range of errors also increased with increasing image noise. In this study, the tracking error gradually increased after about half of the original quantum number. It was actually difficult to identify implanted markers in images generated by less than half of the original incident quantum number. Such information would be very useful for physicists to determine the exposure dose according to the necessary tracking accuracy. The present method could be applied to a different FPD system, requiring only the determination of the conversion function for that system. These results indicated the feasibility of the simulation approach for determination of the exposure dose during real-time target tracking in radiotherapy. The present method would be used as follows: two high-quality images would be taken of a patient during respiration, and then input to the system to simulate images with various levels of image noise. A target would be tracked in two images and the tracking error estimated for each dose level. The results would then allow us to determine the lowest patient dose possible while maintaining tracking accuracy.

There are several limitations for this method. First of all, it has not been generalized enough for clinical use. More imaging parameters and situations need to be considered to provide useful information for clinical practice. In this preliminary study, however, we have demonstrated the feasibility of the simulation approach for determination of imaging conditions based on the relationship between noise level and tracking accuracy. We believe that this simulation approach is one possible way of optimizing imaging conditions. Second, there are the other factors that affect image quality, such as X-ray tube voltage, image lag, image blurring and patient body thickness. In addition, it is necessary to consider the noise factors apart from quantum noise, e.g. electrical noise and structural noise. It should be highlighted in this context that the simulation approach allows us to evaluate the accuracy of target tracking at any noise level. However, all of the noise factors are not involved in the simulation image in the present system. One solution is the adaption of more accurate simulation methods [22–23]. Furthermore, the present system could not demonstrate relationship between exposure dose and noise level. For clinical implementation, further studies are required to expand the system, to install a high-accuracy algorithm for noise simulation and target tracking, and to evaluate it for a real moving target in clinical cases.

CONCLUSION

The present study was performed for the development of a computer simulation method for determining imaging conditions during target tracking in radiotherapy. Image noise was simulated based on the noise property of the system, and the simulation was able to describe the relationship between image noise levels and accuracy of target tracking, in which the maximum tracking error increased with a decrease in the incident quantum number. These results indicated that the simulation approach is one possible method of optimizing imaging conditions.

FUNDING

This work was supported in part by a research grant from the Japanese Society of Medical Physics (JSMP).

REFERENCES

1. Jaffray DA, Siewerdsen JH, Wong JW *et al*. Flat-panel cone-beam computed tomography for image-guided radiation therapy. *Int J Radiat Oncol Biol Phys* 2002;**53**:1337–49.
2. Moore CJ, Amer A, Marchant T *et al*. Developments in and experience of kilovoltage X-ray cone beam image-guided radiotherapy. *Br J Radiol* 2006;**79**:66–78.
3. Huntzinger C, Munro P, Johnson S *et al*. Dynamic targeting image-guided radiotherapy. *Med Dosim* 2006;**31**:113–25.
4. Overdick M, Solf T, Wischmann H-A. Temporal artifacts in flat dynamic x-ray detectors. SPIE medical imaging. *Proc SPIE* 2001;**4320**:47–58.
5. Friedman SN, Cunningham IA. A method to measure the temporal MTF to determine the DQE of fluoroscopy system. In: Flynn MJ, Hsieh J (eds). *Medical Imaging 2006, Proc SPIE* 2006;**6142**:61421X-1–X-11.
6. Friedman SN, Cunningham IA. A small-signal approach to temporal modulation transfer functions with exposure-rate dependence and its application to fluoroscopic detective quantum efficiency. *Med Phys* 2009;**36**:3775–85.
7. IEC. *IEC International standard 62220-1. Medical electrical equipment. Characteristics of digital X-ray imaging devices – Part 1–3*: *Determination of the detective quantum efficiency – Detectors used in dynamic imaging*. Geneva, Switzerland: IEC, 2008.
8. Cremers F, Frenzel T, Kausch C *et al*. Performance of electronic portal imaging devices (EPIDs) used in radiotherapy: image quality and dose measurements. *Med Phys* 2004;**31**:985–96.
9. Berger L, François P, Gaboriaud G *et al*. Performance optimization of the Varian aS500 EPID system. *J Appl Clin Med Phys* 2004;**7**:105–14.
10. McGarry CK, Grattan MW, Cosgrove VP. Optimization of image quality and dose for Varian aS500 electronic portal imaging devices (EPIDs). *Phys Med Biol* 2007;**52**:6865–77.
11. Veldkamp WJ, Kroft LJ, van Delft JP *et al*. A technique for simulating the effect of dose reduction on image quality in digital chest radiography. *J Digit Imaging* 2009;**22**:114–25.
12. van Gelder RE, Venema HW, Florie J *et al*. CT colonography: feasibility of substantial dose reduction–comparison of medium to very low doses in identical patients. *Radiology* 2004;**232**:611–20.

13. van Gelder RE, Venema HW, Serlie IW *et al*. CT colonography at different radiation dose levels: feasibility of dose reduction. *Radiology* 2002;**224**:25–33.
14. Tanaka R, Ichikawa K, Matsubara K *et al*. Review of a simple noise simulation technique in digital radiography. *Radiol Phys Technol* 2012; Online first doi: 10.1007/s12194-012-0152-7 (http://www.springerlink.com/content/5002w618qk982p64/) (25 April 2012, date last accessed).
15. Båth M, Håkansson M, Tingberg A *et al*. Method of simulating dose reduction for digital radiographic systems. *Radiat Prot Dosimetry* 2005;**114**:253–9.
16. Saunders RS, Jr, Samei E. A method for modifying the image quality parameters of digital radiographic images. *Med Phys* 2003;**30**:3006–17.
17. Dainty JC, Shaw R. *Image Science. Principles, Analysis and Evaluation of Photographic-type Imaging Processes*. London, UK: Academic Press, 1974,
18. Huda W. Review of radiologic physics. 3rd edn. Philadelphia, USA: Lippincott Williams & Wilkins, 2010,
19. IEC. *IEC International standard 61267 Medical diagnostic X-ray equipment – Radiation conditions for use in the determination of characteristics*. Geneva, Switzerland: IEC, 1994.
20. ImageJ. *Image Processing and Analysis in Java Version 1.46r*. http://rsb.info.nih.gov/ij/ (date Month year, date last accessed).
21. IEC. *IEC International standard 62220-1. Medical electrical equipment. Characteristics of digital X-ray imaging devices – Part 1: Determination of the detective quantum efficiency.* Geneva, Switzerland: IEC, 2003.
22. Neitzel U, Günther-Kohfahl S, Borasi G *et al*. Determination of the detective quantum efficiency of a digital x-ray detector: Comparison of three evaluations using a common image data set. *Med Phys* 2004;**31**;2205–11.
23. Ballard DH, Brown CM. *Computer Vision*. Englewood Cliffs, NJ: Prentice-Hall, 1982.